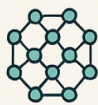# RESEARCH PAPER

Nanoceramic materials for bone regeneration: a systematic review in animal experimental studies

M.A. Cruz[1]; T.A.T. Araújo[1]; I.R. Avanzi[1,2]; G.C.A. Vale[1]; G.E. Santo[1*]; L.C.S. Silva[1]; K.S.J. Sousa[1]; J.R. Parisi[3]; J.L. Merlo[4]; A.R.C. Braga[1]; D.A. Ribeiro[1]; A.C.M. Rennó[1]

*Corresponding author: E-mail address: *giovanna. santo@unifesp.br

NANOCERAMIC MATERIALS FOR BONE HEALING

Data screening

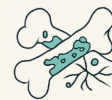162 records identified
↓
127 records excluded
↓
29 studies included
↓
Histological analysis of bone healing

Types of nanoceramics

Hydroxyapatite (HA)
TCP, β-TCP, Calcium phosphate
Bioglass (BG)
Calcium silicate

In vivo results

Increased bone formation
Neoangiogenesis
Marker expression
HCA formation

Isolated or combined nanoceramics have demonstrated efficacy in bone regeneration and are promising for clinical applications in tissue engineering.

Abstract: Nanoceramic materials are used for bone healing. However, the diversity of nanoceramics and the different manufacturing methods used in literature make results difficult to compare. In this context, the purpose of this study was to perform a literature systematic review examining the effects of different nanoceramic materials in bone healing. The search was performed according to Preferred Reporting Items for Systematic Reviews and Meta-Analysis (PRISMA) orientations and Medical Subject Headings (MeSH) descriptors: "bone tissue", "nanomaterial", "ceramic" and "animal studies". 162 articles were retrieved from PubMed and Scopus databases. After elegibility analyses, 29 papers were included (covering a 2007 and 2020 period). Results demonstrated that the commonest materials were Hydroxiapatite, Bioglass, Ttricalcium Phosphate and Bicalcium Phosphate, alone or associated with other materials or drugs. *In vivo* results showed that nanoceramic materials promoted bone healing in different animals models. As conclusion, nanoceramic materials are excellent candidates as bone grafts due to their bioactivity and good bone interaction.

Keywords: Nanoceramic. Nanomaterial. Bone regeneration. Animal studies. Systematic Review.

---

[1]Federal University of São Paulo (UNIFESP), Brazil.
[2]São Paulo State Faculty of Thecnology (FATEC), Brazil.
[3]Metropolitan University of Santos (UNIMES), Brazil.
[4]Applied Electrochemestry Division, Materials Science and Technology Research Institute (INTEMA), National University of Mar del Plata – UNMdP, Argentina.

Introduction

Bone fractures are common injuries caused by traumas and diseases and represent a significant global health burden1. Although most of them have the intrinsic ability of self-repairing, in some specific cases, such as great dimensions bone defects or fractures associated to bone diseases, the healing process can be impaired, leading to an atypical consolidation or non-union fractures[2,3.]

Considering these issues, the development of therapeutical approaches with the aim of stimulating bone repair toward proper consolidation is required[4–7]. Following this line, the use of biomaterials for bone grafting is very promising strategy being capable of stimulating osteoblast cell differentiation and inducing newly formed bone deposition, enhancing healing[4–8].

In this context, many different kinds of materials are used, being the class of bioceramics the most promising[9,10]. It includes a broad range of inorganic and nonmetallic compositions including hydroxyapatite (HA), tricalcium phosphate (TCP) and bioactive glass[2,11,12].

HA is one of the most used ceramic materials, presenting an appropriate ability to stimulate bone tissue repair and lack of citotoxicity[13,14]. In addition, HA promotes newly tissue ingrowth through osteoconduction mechanisms, without causing any systemic or local toxicity, inflammation, or similar responses induced by other foreign bodies 15. Additionally, TCP is another ceramic material used for bone tissue engineering proposals[16,17]. TCP has bioactive properties, it is biocompatible and present a more appropriate index of degradation than HA[17]. Finally, bioactive glasses, with their osteoinductive properties and ability to recruit stem cells and induce their differentiation into bone cells, are considered the most bioactive ceramics[18,19]. Due to these properties, they have been extensively used to repair periodontal bone defects, maxillo-facial defects reconstruction, spinal surgery and bone replacement[19–23].

In addition, ceramic materials have been used at nanosize scale particles, which seems to enlarge the surface area and to make the interfacial interaction stronger, culminating in improved biological performance[23–26]. It has been demonstrated that nanoceramic scaffolds have superior properties such as a more appropriated rate of degradation, allowing newly bone tissue ingrowth[27] and mimicking better the structure and biological function of the extracellular matrix[28].

Figure 1 illustrates some of the scaffold based nanoceramic materials used for bone tissue engineering proposals.
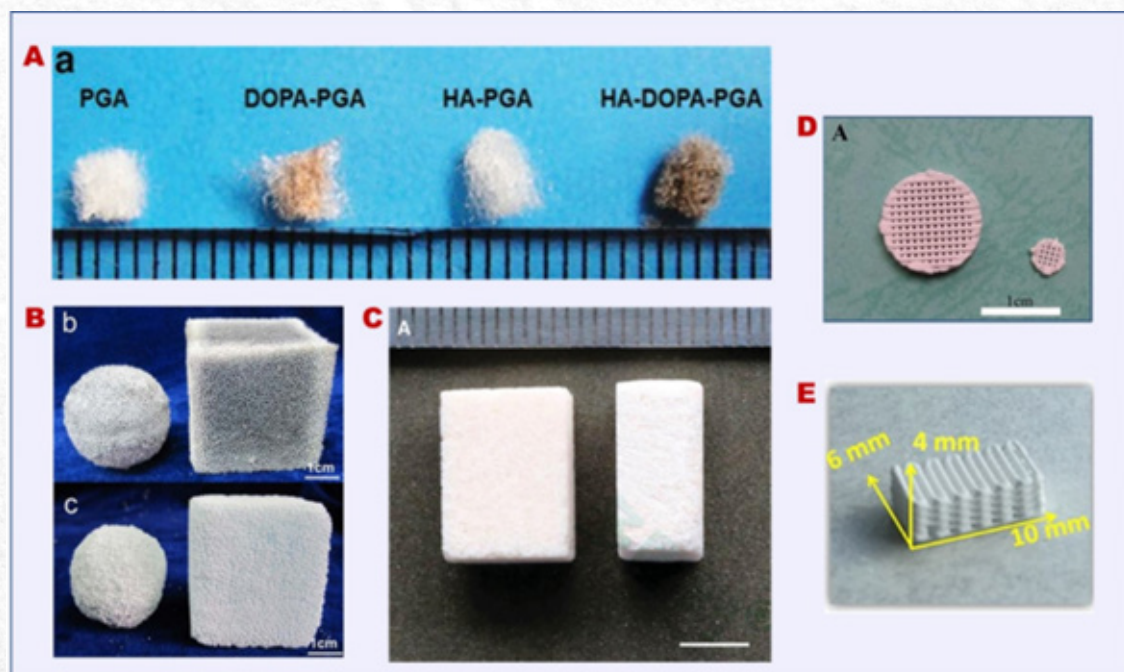

Figure 1. Nanoceramic materials for bone regeneration. A - Macroscopic image of scaffolds Poly-glycolic acid (PGA) 3,4-dihydroxyphenylalanine (DOPA) and HA nanoparticle (PGA, DOPA-PGA, HA-PGA, and HA-DOPA-PGA) by Yang *et al.* (2012). B - Porous calcium carbonate scaffolds by Wang *et al.* (2014). C - Cross-sectional view of the porous nano-hydroxyapatite/coralline block scaffolds by Zhou *et al.* (2015). D - HA scaffolds sintered at various temperatures by Sun *et al.* (2016). E - 3D-printed porous scaffolds by Shao *et al.* (2017).

Despite the evidenced positive effects of nano-ceramic materials on the process of bone healing, there is limited understanding of the biological interactions and mechanisms of action of ceramics materials and bone. Moreover, the different combined protocols used different kind of biomaterials used and huge differences regarding the different methods for material manufacturing (at nanoscale), the diverse material compositions and the diverse animal models used for the different authors, make difficult to compare the results. In this context, the purpose of this study was to perform a systematic review of the literature evaluating the effects of different ceramic nanomaterials for bone tissue healing in in vivo experimental models. Consequently, this work discusses the results for a better understanding of the effects of different therapies in this type of injury.

Methodology
Review protocol

The systematic review was performed according to the SYRCLE guideline by Vries et al.[29] and it was conducted from July to August of 2023 using PubMed and Scopus databases. The search was carried out according to the orientations of Preferred Reporting Items for Systematic Reviews and Meta-Analysis (PRISMA). To start the review, some descriptors of the Medical Subject Headings (MeSH) were defined: "bone tissue", "nanomaterial", "ceramic," and "animal studies". Synonyms in the title and abstract were searched for all the key words (Figure 2).
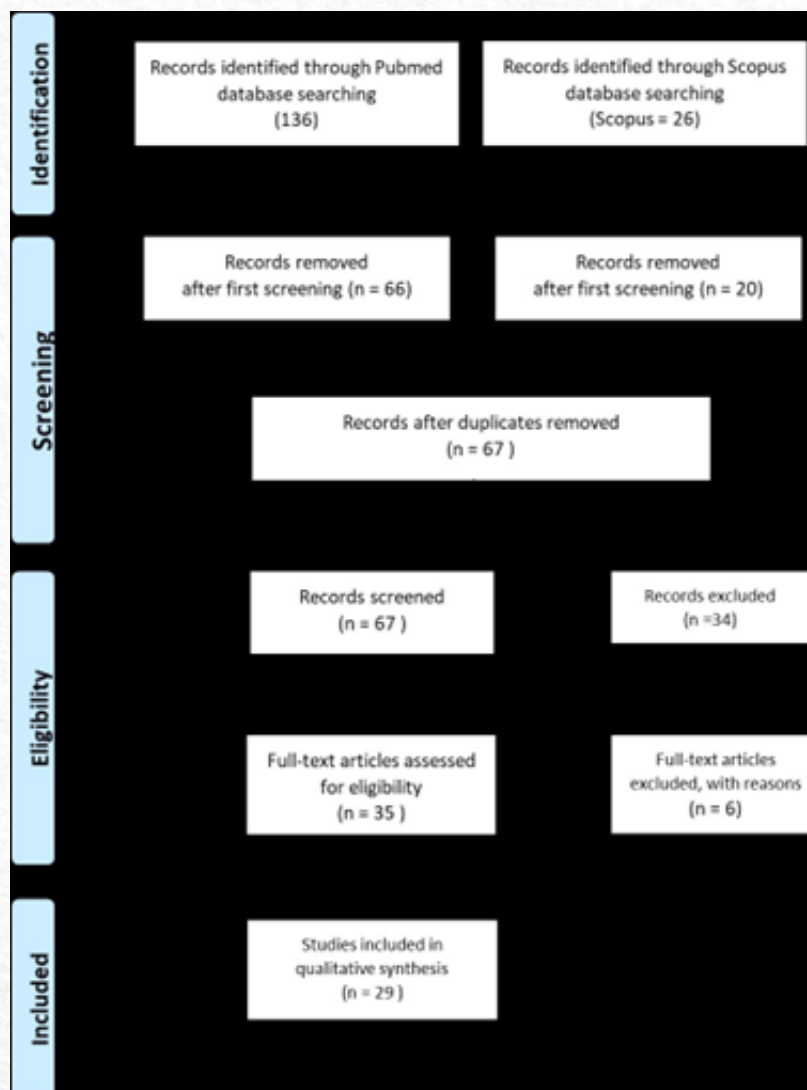

Figure 2. PRISMA flow diagram of the search strategy.

Study selection

Two reviewers (ACMR and MAC) analysed the titles and abstracts of the studies independently and pointed out the studies matching all the inclusion and exclusion criteria. Furthermore, 3 reviewers (ACMR, MAC and TAA) had access to the selected studies to verify the eligibility. Disaccords were solved by discussion. All the chosen studies were further reviewed throughfull-text screening and the studies that have not followed the eligibility criteria were excluded.

Eligibility criteria
Inclusion criteria

1. Animal experiments;

2. Animal studies using bone defects or fractures treated with ceramic materials at nanoscale sizes (used alone or with composites).

3. Articles included by active search in the selected articles' bibliographic reference list and searched in personal archives.

4. Articles in English language and published in the last 20 years.

Exclusion criteria

1. Clinical trials, in vitro studies, in situ studies, reviews, case reports;

2. Studies without bone defects or fractures;

3. Use of non-ceramic materials;

4. Lack of description of the bone fracture or defect, methodology, or outcomes;

5. Animal models with other systemic diseases (such as diabetes, osteoporosis).

Data extraction

The analysed variable was "bone healing", which was based on the histological analysis. In addition, other variables were also extracted: authors names, species/strain, animal sex, age, weight, type of ceramic, use with another material, kind of fracture or defect and size, implantation period (days), way of treatment, material manufacturing, analysis performed in the in vivo studies and outcomes.

Types of Reported Results

Due to the heterogeneity of the primary studies, it was not possible to perform a meta-analysis. To compare the effect size (ES) of treatments, we calculated the normalized average difference, considering the values before and after the intervention. They were further classified as small (< 0.20), moderate (about 0.50), or large (> 0.80), according to Cohen's criteria.

GRADE was used for determining the quality of the papers considering the following domains: trial design limitations due to risk of bias, inconsistency of results, indirectness, imprecision of results and publication bias.

Data synthesis and statistical analysis

The extracted data was presented using the same unit of analysis (%). Furthermore, the effect size as a raw difference in means (MD) of new bone formation (%) was calculated with a 95% confidence interval (CI).

Results

The flow diagram demonstrates the search strategy used in the present study (Figure 1). A total of 162 articles was retrieved from the databases (PubMed and Scopus). From those, 78 works were selected for the first screening. The duplicated records were excluded (n = 71). Two independent researchers screened the 71 articles and 37 studies were excluded due to the lack of criteria attendance. Thus, 35 full-text articles were assessed for eligibility and, from them, 6 studies were excluded for presenting only non-ceramic bone substitutes. Finally, 29 studies were included and analyzed in the present systematic review.

Table 1 shows the characteristics of all included in vivo studies such as the type of nanoceramic used for bone repair, species/strain, animal sex, age, weight, nanomaterial, surgery site, bone defect size, implantation period (days) and way of treatment.

Different animal models were used in the studies. Sixteen of them used rabbits as an experimental model[28,30,39–43,31–38], 13 studies used rats[25,44–52], 3 studies used dogs as an experimental model[26,53,54] and only 1 work studied the material effects in ovine bone defect model[55] (Table 1).

Furthermore, 15 studies performed the bone defect in the forelegs of animals as described: 6 performed in the middle femur[32,47,54,56], 4 performed in the tibia[30,33,48,50], 1 performed in the femoral trochanter [57], 3 performed in the femoral condyle[38,39,55] and 1 study just described as foreleg cortical bone [42]. In addition, 8 studies used the calvaria to perform the bone defect[25,37,44–46,49,52], 4 used the mandible[26,28,51,53], 2 used the iliac bone[40,41] and 2 used the radius[31,34].

The size of the bone defects varied from 1 mm to 15 mm in diameter[25,26,40,41,44–46,48–52,30,53–55,57,58,31,33,34,36–39].

In addition, distinct time points were analysed with the minimum experimental period of 7 days [49] and the maximum experimental period of 112 days (16 weeks)[28].

An overview of bioactive nanoceramic materials, the drugs and biomaterials used for composite scaffolds manufacturing, as well as the physicochemical characteristics of ceramic nanobiomaterials are exhibited in Table 2.

From Table 2, it is possible to observe that in this

systematic review, HA was the most common nanoceramic used by the authors, being used in the form of composites that were tested in 13 studies. Dasgupta et al.[30](2019) studied HA combined with β-tricalcium phosphate (β-TCP) and bioactive glass as nanoceramic materials, and chitosan and gelatin as natural polymers, Chalisserry et al.[38](2019) studied nanohydroxyapatite (nHA) with Simvastatin, Rogowska-Tylman et al.[41](2019) studied nHA combined with β-TCP and Polycaprolactone (PCL), Ahmadzade et al. 33(2016) tested composites of carbonate hydroxyapatite (cHA) combined with Polyvinyl alcohol (PVA) and zinc-magnesium ions, Sun et al. [46](2016) manufactured nHA scaffolds, loaded with bone morphogenic protein 2(BMP-2)-related peptide (P28), Dhivya et al.[48](2015) studied nHA blended with zinc-doped chitosan (Zn-CS) and beta-glycerophosphate (β-GP), Hu et al.[31](2015) manufactured nHA scaffolds with biphasic calcium phosphate (BCP), Zhang et al.[39](2015) tested HA, amorphous calcium phosphate (ACP) nanospheres and Poly (D, L-lactic acid) (PLA) composites, Zhou et al.[14](2015) studied nHA combined with coralline (coral) and recombinant human vascular endothelial growth factor (rhVEGF165), Wang et al.[34](2013) prepared nHA and poly (lactic-co-glycolic acid) (PLGA) scaffolds, Reddy et al.[47] (2012) tested HA and β-TCP scaffolds with mesenchymal stem cells (MSCs), Yang et al.[52](2012) manufactured HA comgined with Polyglycolic acid (PGA), while Huber et al.[42](2007), tested composites manufactured with HA commercially available OSTIM® and CERABONE®.

Moreover, 8 studies explored the calcium phosphate as nanoceramic material as described: Rezaei et al.26(2018) and Zhu et al.[54](2017) tested only BCP nanoceramic scaffolds, Kazemi et al.[37](2019) studied β-TCP combined with bioglass (BG), strontium, and polyvinyl alcohol (PVA), Shao et al.[28](2017) tested β-TCP with calcium silicate (CaSiO3 / CSi), magnesium (Mg); bredigite (Bred) and PVA scaffolds, Bennett et al.[55](2016) manufactured α–TCP with Poly (D, L-lactide-co-glycolide) (PLGA), Lysenko et al.51(2015) studied BCP combined with BG and Silver - Cooper ions, Wang et al.[32](2014) studied nano calcium phosphate ceramic with gelatin, while Zhou et al.[56](2014) mixture amorphous calcium phosphate (CaP) with PLA and Tantalum (TA).

In addition, in the current systematic review, 5 studies investigated the effects of BG at nanoscale as follow: Singh et al.[40](2019) combined Nanobioglass (nBG) with chitosan (CH) and chondroitin sulfate (CS), Lisboa-Filho et al.[25](2018) proposes to evaluate the biological potential of BioGran® combined with Raloxifene, Zhang et al. (2018) 28 fabricated nBG mixture with Polyetheretherketone (PK), Johari et al.[49](2016) tested 64S-BG powder and gelatin composites, while Ardeshirylajimi et al.44(2015) studied BG scaffolds, coated with Polyethersulphone (PES) nanofibres.

Furthermore, the biological effects of bioactive silicate nanoceramic materials can be found in 3 studies: Liang et al.[45](2019) manufactured mesoporous silica (MSNs) with gold nanoparticles (AuNP) scaffolds, Mabrouk et al.[50](2018) combined calcium silicate nanoparticles with copper and silica gel, while Razavi et al.[57](2015) studied bioactive silicate akermanite (Ca2MgSi2O7) with magnesium alloy.

Regarding the scaffold fabrication process, it was possible to observe that a wide variety of methodologies were applied. The chemical precipitation method was carried out by four studies[50,51,54]. This chemical analytical route has general advantages such as superior uniformity and high yield of nanoparticles[59].

Due to the possibility of large-scale productions combined with the simplicity of the process, electrospinning is one of the most employed techniques in biomedical field applications, like tissue engineering drug release and wound dressing60. In this systematic review, the electrospinning technique was applied in two studies[39,44] and one study involved electrophoretic deposition[57], while two studies used the leaching method[28,34].

One study manufactured scaffolds by the replication method37, and in the researches by Wang et al.[32](2014) and Sun et al.[46](2016), the scaffolds were fabricated through sintering process, while two studies applied freeze-drying and gelation methods[40,49]. The sonochemical and ultra-sonification methods were utilized in two studies[25,41].

Three-dimensional (3D) printing is becoming an increasingly common technique to fabricate scaffolds and devices for tissue engineering applications due, among others, to it can provide patient-specific design, highly structural complexity and rapid on-demand fabrication at a low-cost[61], being applied in this review by Shao et al.[62](2017) for scaffold fabrication. The remaining studies utilized a variety of chemical analytical techniques such as hydrolyzing in alkaline solution and wet chemical methods.

In adittion, the physical, chemical and morphological characteristics of the samples are shown in Table 2. The scanning and transmission electron microscopy was used in 18 studies and showed the porosity, interconnected network, and surface microstructure of the scaffolds[28,32,48–52,54,56,63,34,35,37,39–41,46,47] and four studies used the Fourier Transform Infrared Spectroscopy (FTIR) for the chemical characterization[26,31,33,55].

Table 3 shows the in vivo analyses, results and outcomes of the studies. Among them, 21 performed image analysis such as X-ray[30,33,44,47,48,50,54,55]

and microtomography (micro-CT)[25,33,34,37,38,44–46].

The authors observed that nanosized materials were able of inducing bone growth and increasing bone density in the region of the defects and fractures[25,26,46,48,50,52,54,55,57,30,32–34,37,38,44,45].

Twenty-five studies performed a qualitative histological analysis. Among them, 3 authors found interaction between the implant and bone tissue [33,42,47], 5 found a progressive degradation of the implanted materials[28,30,32,38,55], 23 found a higher amount of newly formed bone tissue at the region of the defect in the biomaterial treated animals [26,,28,44–50,52,54,55,31,56,57,63,32–34,37,39,41,42]. In addition, reduced or absent inflammatory reaction to implanted materials was observed by Lysenko et al.[51](2015), Razavi et al.[57](2015), Rezaei et al.[26] (2018), and Shao et al.[28] (2017). At the same time, migration of bone cells to the treated zone were observed by Sun et al.[46](2018), and collagen deposition as well as presence of mineralized bone matrix was found by Ardeshirylajimi et al.[44](2015), Dhivya et al.[48] (2015), Singh et al.[40] (2019), and Zhang et al.[39](2015). Mabrouk et al.[50] (2019), Sun et al.[46] (2018). Du et al. [53] (2015) also observed increased angiogenesis in implanted animals.

In addition, quantitative histological analysis has been performed by 10 authors and as a result, they observed higher bone formation[26,31,37,38,41,42,49,52], higher index of angiogenesis[53], higher implant degradation[26,41,49] and lower fibrous connective tissue formation[26,37,41] in treated animals.

Seven articles performed immunohistochemistry analysis and as a result demonstrated that the nanoceramic materials produced an increase in the immunostaining of osteogenic markers as osteocalcin (OCN)[37,41,49], bone morphogenic Protein-2 (BMP-2)[31,41,46,] Vasoendothelial Growth Factor (VEGF)53 and Collagen type-I[45]. The study performed by Rogowska-Tylman et al.[41](2019) also found increased immunostaining of Osteoprotegerin (OPG), Osteopontin (OP), Matrix Metalloproteinase-2 (MMP2), Tissue Inhibitor of Matrix Metalloproteinase (TIMP2), Interleukin-1 (IL1), and interleukin 10 (IL10).

Some complementary analysis were performed by the studies conducted by Dasgupta et al.30(2019), Zhu et al.[54] (2017), Ahmadzadeh et al.[33] (2016), Hu et al.[31] (2015) and Wang et al.[34](2013). Hu et al.[31] (2015) and Zhu et al.[54](2014) performed mechanical tests and found an increase in the maximum flexural strength (N), load (N), and stiffness (N/mm), respectively. Dasgupta et al.[30] (2019) performed a fluorochrome labeling and observed the bone growth ratio of 70.450% in the bioglass group after 3 months. Wang et al.[34] (2013) also performed fluorochrome labeling and found a bone growth ratio of 3.7 ± 0.3 μm/day. Ahmadzadeh et al.[33](2016) also performed

Scanning Electron Microscopy/Energy Dispersive X-ray (SEM/EDX) analysis to evaluate surface conditions of implantation site and found an increase of Ca/P wt.% ratio of about 1.46% to 1.76% after 4 weeks.

The quality of evidence for nanoceramic materials and bone healing according to the GRADE approach is presented in Table 4. The evidence synthesis was moderate for all experimental studies for the variable histological analysis, demonstrating the efficacy of techniques on the bone repair treatment.

Table 1. *In vivo* studies using nanoceramic biomaterial in bone repair.

Authors and year	Species/ Strain	Ani-mal sex	Age	Wei-ght	Surgery site	Defect size	Implan-tation period	Experimental design
Dasgupta *et al.* (2019)	New Zealand white rabbit	Both	12-15 months	1.5-2 kg	Femur	$2\times2\times5\ mm^3$	3 months	Four groups: GC scaffold (control), GC-HA, GC-β-TCP, and GC-58s BioGlass scaffolds.
Chalisserry *et al.* (2019)	New Zealand white rabbit	*	6-9 months	3.5-5 kg	Femur (condyle)	5 x 8 mm	8 weeks	Defects filled with nHA particles or nHA with Simvastatin.
Kazemi *et al.* (2019)	New Zealand white rabbit	Male	5-6 months	2.5 kg	Cranial bone	Four holes of 0.8 mm diameter	2 and 5 months	The 4 defects were filled with the different materials in the same animal: 50Sr-TCP/50BG scaffold 50Sr-TCP/50BG scaffold loaded with MSCs, HA/TCP granules (positive control), and untreated (negative control).
Liang *et al.* (2019)	Sprague–Dawley rats	Male	10 weeks	250 ± 25 g	Cranial bone	5 mm diameter	4 and 8 weeks	Three animal groups: nanosphere-loaded chitosan scaffolds (CS), MSNs-modified CS, and Au-MSNs modified CS.
Rogowska--Tylman *et al.* (2019)	Rabbit	Male	6 months	*	Iliac bone	5 mm diameter	3 months	Three animal groups: HA-coated β-TCP scaffold, uncoated β-TCP scaffold, and nHA-coated poly-ε-caprolactone scaffold.
Singh *et al.* (2019)	Rabbit	*	*	*	Iliac bone	3-4 mm diameter	6 months	Two animal groups: CH/CS/8nBG scaffold and untreated defect (control).
Lisboa-Filho *et al.* (2018)	Wistar rats	Male	3 months	~250 g	Cranial bone	5 mm diameter	30 days	Three animal groups: defect filled with 100% of BioGran®, 90% BioGran® and 10% raloxifene, and 80% BioGran® and 20% raloxifene.
Mabrouk *et al.* (2018)	Wistar rats	Male	adult	180-200 g	Tibia	Fracture induced	10 days	Five animal groups: a paste of 0%, 1%, 3%, or 5% Cu-doped calcium silicate nanoparticles applied circumferentially around the fracture and untreated fracture (control).
Rezaei *et al.* (2018)	Iranian mongrel dogs	*	*	*	Mandible	3 holes of 8 mm diameter	8 weeks	Defects filled with commercial BCP (positive control), other with nanosized BCP, and others left empty (negative control) in the same animal, bilaterally.
Zhang *et al.* (2018)	New Zealand white rabbit	*	8 months	~4 kg	Femur	5 mm diameter	1 and 3 months	Four animal groups: defect filled with micro-macroporous PK, BPC (control composite of macroporous nBG and PK), mBPC, and mBPC loaded with HK.
Shao *et al.* (2017)	New Zealand white rabbit	Male	*	*	Mandible	$10\times6\times4\ mm^3$	8 and 16 weeks	Four animal groups: β-TCP group (positive control); wollastonite (positive control), wollastonite with Mg (CSi-Mg10), and bredigite (positive control).
Zhu *et al.* (2017)	Beagle dogs	Male	10 months	9.6 ± 0.8 kg	Femur	12 mm long (segmental defect)	12 weeks	Two animal groups: hBCP scaffolds or BCP scaffolds (traditional smooth-surface; control). A stainless-steel plate with 4 screws was used to stabilize the segmental defect.

►►

Table 1. *In vivo* studies using nanoceramic biomaterial in bone repair (cont.).

Ahmadzadeh *et al.* (2016)	New Zealand white rabbit	Male	14 weeks	2 ± 0.2 kg	Tibia	2 holes of 4 mm diameter × 2 mm depth	14, 21, and 28 days	Two animal groups: defects filled with Zn-Mg-HA orHA scaffolds.
Bennett *et al.* (2016)	Welsh Mountain ewe		2-5 years	30-50 kg*	Femur (condyle)	6 mm diameter × 12 mm deep	6, 12, 18, and 24 weeks	PLGA and PLGA/TCP composites containing micro- or nano-sized α-TCP were randomly implanted.
Johari *et al.* (2016)	Wistar rats	Male	*	200-250 g	Cranial bone	8 mm diameter	7, 30, and 90 days	Three animal groups: untreated defect (control), defect filled with bioglass/gelatin scaffold, and osteoblasts/bioglass/gelatin scaffold.
Sun *et al.* (2016)	Sprague-Dawley rats	Male	7-8 weeks old	*	Cranial bone	5 mm diameter	6 and 12 weeks	Four animal groups: untreated defect (control), porous nHA scaffolds without P28 or BMP2, nHA + P28, and nHA+ BMP2 scaffolds.
Ardeshiry-lajim *et al.* (2015)	Rats	Male	*	300 ± 5 g	Cranial bone	8 mm diameter	8 weeks	Three animal groups: PES scaffolds, BG-coated PESscaffolds, and untreated defect (control).
Dhivya *et al.* (2015)	Wistar rats	Male	3 months	200-250 g	Tibia	3 mm diameter	14 days	Three animal groups: untreated defects(control), defect filled with Zn-CS/β-GP, or Zn-CS/β-GP/nHA.
Du *et al.* (2015)	Beagle dogs	Male	12-15 months	12.1 kg ± 0.5	Mandible	Chronic type-defects (box-shaped): 9 × 6 × 12 mm after tooth extraction, allowed to heal for 2 months and then reshaped.	3 or 8 weeks	Two animal groups: nHA/coral block scaffold and VEGF/nHA/coral block scaffold.
Hu *et al.* (2015)	New Zealand white rabbit	Male	*	~2.5 kg	Radius	1.5 cm length (segmental defect)	12 weeks	Four animal groups: defect filled with porous BCP ceramic, nHA-coated porous BCP ceramic, porous BCP ceramic seeded with MSCs, and nHA-coated porous BCP ceramic seeded with MSCs.
Lysenko *et al.* (2015)	Wistar rats	Female	12 months	330 ± 15 g	Mandible	4 mm diameter	10 and 30 days	Four animal groups: intact rats (physiological control), untreated defect (control), defect filled with BG and BCP ceramic, or with BG and BCP ceramic doped with 1% silver and 0.5% copper.
Zhang *et al.* (2015)	New Zealand white rabbit	*	adult	3 kg	Femur (condyle)	5 mm wide	12 weeks	Three animal groups: defect filled with ACP-PLA or HA-PLA composite nanofibers, and untreated defect (control).
Razavi *et al.* (2014)	Rabbits	*	adult	~3 kg	Femur (greater trochanter)	3 mm diameter	2 weeks, 1 month and 2 months	Three animal groups: defect treated with magnesium alloy, with PEO coated magnesium alloy, and with akermanite/PEO coated Mg alloy.
Wang *et al.* (2014)	New Zealand white rabbit	Male	*	3-4 kg	Femur	5 mm diameter	1,2 and 3 months	Defect treated with porous nanoapatite scaffolds. No controls.

►►

Table 1. *In vivo* studies using nanoceramic biomaterial in bone repair (conc.).

Zhou *et al.* (2014)	New Zealand white rabbit	Male	*	*	Femur (condyle)	5 mm wide	12 weeks	Two animal groups: defects treated with VEGF/TGF containing CaP-PLA scaffolds or untreated defect (control).
Wang *et al.* (2013)	New Zealand white rabbit	Male	5 months	2.5-2.9 kg	Radius	15 mm length (segmental defect)	4, 8, 12 weeks	Three animal groups: defect treated with nHA coated PLGA scaffolds with BMSCs or PLGA scaffolds with BMSCs, and untreated defect (control).
Reddy *et al.* (2012)	Wistar rats	Female	3 months	150-200 g	Femur	5 mm diameter	3 months	Three animal groups: defect filled with nanoceramic powder with MSCs, nanoceramic powder without MSCs, and untreated defect (control).
Reddy *et al.* (2012)	Wistar rats	Female	3 months	150-200 g	Femur	5 mm diameter	3 months	Three animal groups: defect filled with nanoceramic powder with MSCs, nanoceramic powder without MSCs, and untreated defect (control).
Yang *et al.* (2012)	Mice	Female	6 weeks	*	Cranial bone	Two holes of 4 mm diameter	8 weeks	Four animal groups: defect treated with PGA scaffolds, DOPA-coated PGA scaffolds, PGA scaffolds immersed in HA solution, and HA- and DOPA-coated PGA (HA-DOPA-PGA) scaffolds.
Huber *et al.* (2007)	Rabbits	*	*	*	Foreleg (ulna)	7 mm length × 5 mm depth	2 months	Four animal groups: defect filled with Cerabone, Ostim, Ostim-Cerabone combination, and untreated defect (control). Two titanium screws ensured the stability of the defect.

Table 2. Bioactive nanoceramic, composite material, the method for scaffold manufacturing and physicochemical characteristics of nanoceramic materials.

Author	Bioactive nanoceramic	Composite material	Method for scaffold manufacturing	Physico-chemical and morphological properties
Dasgupta *et al.* (2019)	HA; β-TCP; 58s bioactive glass (60% SiO_2,36% CaO;4% P_2O_5).	Chitosan (C); Gelatin (G).	The G-C-HA scaffolds (GCH30) were prepared by mixing HA and C nanopowders with G solution (ratio 30:40:30 respectively). The β-TCP nanoparticles were added to G-C solution (ratio 30:40:30 respectively) to prepare GCT30 scaffolds. For the GCB30 scaffolds, the 58S bioactive glass nanoparticles were mixed with G-C solution (ratio 30:40:30, respectively).	The compressive strengths of the scaffolds were in the range between 1-4 MPa (GCH30: 3.45 ± 0.04; GCT30: 2.47 ± 0.02; GCB30: 2.24 ± 0.01, while the scaffolds porosity varied between 78–89% (GCH30: 78.12 ± 3.2; GCT30: 83.11 ± 8; GCB30: 81.08 ± 6), and pore sizes were: GCH30: 94 ± 6.9; GCT30: 120 ± 6.4; GCB30: 100 ± 8.6.
Chalisserry *et al.* (2019)	nHA	Simvastatin (SIM)	SIM was hydrolyzed by adding in an alkaline solution of ethanol/NaOH and heating at 50 °C for 2 h. Hydrolyzed SIM was dropped onto nHA under sterile conditions to incorporate 0.125 mg of SIM on 60 mg nHA, and dried in a laminar flow hood for 24 h.	nHA utilized had a particle size less than <200 nm.
Kazemi *et al.* (2019)	45S5 BG; Strontium substituted (β-TCP)	PVA	Scaffolds were prepared through the foam replication method. PVA was dissolved in deionized water at 80 °C, followed by adding a different proportion of Strontium substituted β-TCP (Sr.TCP) and 45S5 BG nanopowders (Sr.TCP/BG: 100/0, 75/25, 50/50, and 25/75). Polyurethane foams were impregnated, compressed to remove extra uptake, and dried in an oven. The scaffolds were heated up to 350 °C and maintained for 30 min to decompose the foams, and then heated up to an elevated temperature (1250 °C) to sinter and densify the ceramic network.	The Scanning Electron Microscopy (SEM) revealed the highly interconnected porous structure in the scaffolds with porous diameters in the range of 100–500 µm. Porosity in the range of 68–74%.

Compressive strength increased with increasing the BG content. |
| Liang *et al.* (2019) | Mesoporous silica nanoparticles (MSNs) | Gold nanoparticles (AuNP) | MSNs nanoparticles were produced by a solution of hexadecyltrimethylammonium bromide in deionized water, NaOH, and tetraethyl orthosilicate dissolved in methanol. The MNSs was then obtained by centrifugation, calcined, and dissolved in methylbenzene, and a reflux condensation was conducted at 80 °C after the addition of N-(amino-ethyl)-amino-propyl trimethoxy silane. Finally, MSNs were centrifuged, dried, and mixed with an AuNP suspension of 0.125%. | The diameter of nanoparticles in the MSNs and Au-MSNs was about 80–110 nm. A well-aligned mesoporous structure was the typical structure seen in the MSNs. The morphology of the Au-MSNs showed the gold nanoparticles with a diameter of 15 nm distributed across the surface of the MSNs. |
| Rogowska-Tylman *et al.* (2019) | nanohydroxyapatite (nHA); β-tricalcium phosphate (β-TCP) | PCL | β-TCP scaffolds were prepared from calcium-deficient hydroxyapatite (CDHAP). The Poly-ε-caprolactone (PCL) scaffolds were fabricated by using a 3D printer method. Both scaffolds were sonocoated (using high intensity power ultrasounds) with nHA, rinsed with distilled water, and dried. | The SEM images of PCL and β-TCP scaffolds showed an organized structure of fibers and a polycrystalline β-TCP material with a grain size of a few microns and pores with diameters in the range of 20–200 µm. β-TCP sample overall porosity was 49%; average β-TCP pore size was 205 µm, and pore wall thickness was 97 µm. For the 3D-printed PCL scaffold, porosity volume was 41.2%, and mean pore diameter was 420 µm. |

Table 2. Bioactive nanoceramic, composite material, the method for scaffold manufacturing and physicochemical characteristics of nanoceramic materials (cont.)

Singh *et al.* (2019)	Nanobioglass (nBG)	Chitosan (CH); Chondroitin Sulfate (CS)	CH/CS/nBG scaffolds were fabricated through the freeze gelation method. The nBG powder was dispersed in water by sonication. The pH was adjusted (≤3), and then CH was dissolved, stirred overnight, and chondroitin sulfate was then added. The solution was frozen, immersed in a NaOH/ethanol solution, rinsed with ethanol, and washed with PBS. Finally, scaffolds were cross-linked and dried.	The Field emission scanning electron microscope (FE-SEM) images show the average pore size in the range of 170-540 μm, lower with increasing nBG content and uniform distribution of nBG across the scaffolds with a porosity range of 65–75%. Incorporation of nBG shows ~6 fold improvement in compressive strength in comparison with CH/CS based scaffold.
Lisboa--Filho, *et al.* (2018)	BioGran® (BioGran, Inc., USA; bioactive glass)	Raloxifene	The composites of BioGran® and raloxifene in solid form were homogenized by the sonochemical method. Ultra-pure water was used as a medium to obtain a homogeneous mixture and decreasing particle size.	
Mabrouk *et al.* (2018)	Calcium silicate nanoparticles	Copper (Cu); Silica gel	The Cu doped calcium silicate powders were synthesized utilizing the wet precipitation method. Calcium nitrate solution was obtained by dissolving calcium carbonate in nitric acid, and silica gel powder was added to obtain the calcium silicate gel. Cu nitrate solution was obtained by dissolving Cu carbonate separately in nitric acid and then titrated onto the calcium silicate gel to obtain a homogeneous mixture gel. The formed gel was dried at 100 °C, calcined up to 550 °C, milled, and sieved from a 63 μm standard sieve.	The TEM images showed nanoscale size rounded grains of ~ 50 nm. The Cu-free sample showed irregular agglomerated particles with a particle size range of 12–36 nm, and the samples containing 3% and 5% Cu showed interconnected fine particles in the range of 13–28 nm.
Rezaei *et al.* (2018)	Biphasic calcium phosphate (BCP) ceramic	–	A commercial BCP composed of 70% HA and 30% β-TCP was dry-milled in a high energy planetary ball mill with zirconia balls and containers for 6, 12, 18, 20, and 30 hours at a speed of 530 round per minute.	The FTIR spectrum of the nano-biphasic calcium phosphate (BCP) reveals the hydroxyl, phosphate, and carbonate groups. The longer the milling time, the smaller the particle size. BCP particles had a roughly spherical shape of 100 nm.
Zhang *et al.* (2018)	Nano-bioglass (nBG)	Polyethere-therketone (PK)	The Nano-bioglass (nBG) / Polyetheretherketone (PK) scaffolds were fabricated using the cool-pressed sintering and particle leaching method. The nBG and PK powders were dispersed in sodium chloride saturated solution. The mixture was put into the molds and pressed under a load of 40 MPa, and sintered. The porous scaffolds were obtained after their immersion in deionized water to remove NaCl particles, followed by drying.	The SEM images of the scaffolds' surface morphology showed macroporous (of about 400 μm) and micropores (of about 10 μm). The scaffold had a porosity of 72.5%, water absorption of 450.4 %, and compressive strength of 3.3 MPa.
Shao *et al.* (2017)	Calcium silicate (CaSiO₃ / CSi); β-trical-cium phosphate (TCP)	Magnesium (Mg); Bredigite (Bred); Polyvinyl alcohol	Calcium silicate (CSi) and CSi-Magnesium (Mg) powders were synthesized by a chemical co-precipitation method. β-tricalcium phosphate (TCP) and Bredigite (Bred) powders were synthesized by wet-chemical and sol-gel processes. The powders were ground in ethanol, and the paste was prepared by mixing bioceramics powders with a polyvinyl alcohol solution, and the 3D printing technique manufactured the scaffolds.	The SEM showed that the bioceramic scaffolds were all composed of superfine particles with a size below 3 μm, and the X-Ray diffraction (XRD) patterns confirmed the crystallinity in the scaffolds. The new scaffold of ~10% Mg-substituted wollastonite developed presented a pore size of 313 ± 19.1 μm and porosity of 51.2 ± 4.6 %.

►►

Table 2. Bioactive nanoceramic, composite material, the method for scaffold manufacturing and physicochemical characteristics of nanoceramic materials (cont.).

Reference	Bioactive nanoceramic	Composite material	Method	Physicochemical characteristics
Zhu *et al.* (2017)	Biphasic calcium phosphate (BCP) bioceramics	–	The Biphasic calcium phosphate (BCP) nanoparticle slurry and BCP powders were synthesized by a chemical precipitation method. The porous BCP ceramic scaffolds were then fabricated using the H_2O_2 foaming method and sintered at 1100° C for 2 h. The scaffolds were then modified via hydrothermal treatment and washed. The prepared BCP nanoparticle slurry was adsorbed into the scaffolds by vacuum infusion, dried, and then sintered at 1100 °C. The above infusion step was repeated with a half-reduced slurry concentration and then sintered at 1000 °C to obtain a micro/nano hybrid-structured BCP bioceramic.	The SEM image indicated that the micro/nanohybrid-structured BCP scaffold surface presented a micro-whisker network filled with thick layers of BCP nanoparticles, mainly residing on the whiskers' root and top.
Ahmad-zade *et al.* (2016)	Carbonate hydro-xyapatite (cHA)	Enterobacter aerogenes (PTCC 1221); Polyvinyl alcohol (PVA); magnesium (Mg^{2+}) and zinc (Zn^{2+}) ions	For the composite graft fabrication, polyvinyl alcohol (PVA) was dissolved in distilled water. cHA and Zn-Mg-HA mixed powder was added. After dissolving the mixture, the temperature was raised to 100 °C and kept at this condition for 30 min. The composites were cut into small disc shaped pieces and sterilized by autoclaving.	The FTIR demonstrated all characteristic absorption peaks regarding the functional groups of Carbonate hydroxyapatite (cHA), including PO_4^{3-} (PO), OH^- (O-H), and CO_3^{2-} groups (C-O).
Bennett *et al.* (2016)	Tricalcium phos-phate (α -TCP)	Poly (D, L-lactide-co-glycolide) (PLGA)	The scaffolds were produced by dispersing α-TCP powder in acetone, followed by the gradual addition of PLGA pellets. The mixture was stirred to obtain a micro-sized material or attritor-milled to produce a nano-sized material.	Most of the particles were~1 μm in micro-sized material and ~ 0.1-0.5 in nano-sized material.
Johari *et al.* (2016)	64S -Bioactive glass powder (64% SiO_2, 31%CaO, 5%P_2O_5)	Gelatin	The bioactive glass/gelatin (40/60 wt %) nanocomposite was fabricated by layer solvent casting combined with freeze-drying and lamination techniques. The nanocomposite scaffolds were soaked in 1% (w/v) glutaraldehyde solution for 24 h to cross-link gelatin polymeric chains.	SEM images demonstrated the porosity of about 85%, and the average pore size of the scaffolds was in the range of 200 to 500 μm.
Sun *et al.* (2016)	Nano-hydro-xyapatite (nHA)	Bone morphogenic protein 2(BMP-2)-related peptide (P28)	nHA scaffolds were sintered in a chamber furnace (pre-sintered at 400 °C for 1 h and then sintered at 1000, 1100, 1200, 1300, or 1400 °C) for 2 h, sterilized in 70% ethanol, washed with deionized water, and dried naturally overnight. 3 mg of bone morphogenic protein 2(BMP-2)-related peptide (P28) was dissolved in deionized water and dropped on the scaffold. The scaffolds were dried in a vacuum drying oven, frozen, and sterilized with 70% ethanol.	SEM showed interconnected pores, homogeneously dispersed in the nHA scaffolds when the sintering temperature was below 1200 °C, and no pores were observed when the sintering temperature was above 1200 °C. Compressive strength increased with increases in sintering temperature, whereas porosity, water absorption, and controlled release of loaded peptides decreased as the sintering temperature increased. Sintering at 1000 °C produced the optimal properties for cell responses.
Ardeshiry-lajimi *et al.* (2015)	BG	Polyethersulphone (PES) nanofibres	The electrospinning method was used to fabricate bioceramic coated PES nanofibrous scaffolds. Plasma treatment was used to increase the hydrophilicity of PES surfaces. The PES nanofibrous scaffolds were immersed in BG /distilled water overnight and sterilized.	The PES scaffolds had a porous structure with smooth morphology, nanofiber diameters between 311 and 569 nm, and contact angle reduced to zero. PES nanofibers had a tensile strength of 0.97 ± 0.1 MPa and elongation at a break of 36.01 ± 2.7%.

►►

Table 2. Bioactive nanoceramic, composite material, the method for scaffold manufacturing and physicochemical characteristics of nanoceramic materials (cont.)

Dhivya *et al.* (2015)	Nano-hydro-xyapatite (nHA)	Zinc-doped chitosan (Zn-CS); beta-glycerophosphate (β-GP)	Zn-CS/β-GP and Zn-CS/β-GP/nHA solutions were prepared by drop-wise addition of an optimized molar concentration of pre-cooled β-GP to pre-cooled solutions of Zn-CS and Zn-CS/nHAp under continuous mixing. The hydrogel formed at 4°C was transferred to 37 °C for gelation. The hydrogel was then stored at -20 °C overnight, followed by lyophilization.	SEM analysis of the Zn-CS/β-GP and the Zn-CS/β-GP/ nHAp/ revealed porous architectures indicative of the presence of both micro and macro-sized pores, with uniformly interconnected patterns with diameter in the range of 100–150 μm.
Hu *et al.* (2015)	Biphasic calcium phosphate (BCP); Nano-hydroxyapatite (nHAp)	–	A hydrothermal deposition method was applied to prepare the nHA for coating the BCP scaffolds. Polyvinylpyrrolidone was added to the ammonium dihydrogen phosphate solution. Next, the BCP and calcium nitrate tetrahydrate was added to the solution. The continuous ultrasound was applied, and the product was moved to a hydrothermal synthesis reactor under hydrothermal conditions (120 C° and 12 h). The nHA-coated porous BCP scaffolds were removed and filtered.	FTIR showed that the nHA was successfully incorporated in BCP scaffolds. The porosities of the two ceramics were at approximately 50.5 ± 1.3 and 50.2 ± 1.1 % for BCP and nHA-coated BCP scaffolds, respectively. Macropores of 150 to 500 μm containing many micropores (< 10 μm) were observed in the BCP scaffolds.
Lysenko *et al.* (2015)	Bioactive glass ceramic (BG) ($37SiO_2$–$36CaO$–$13P_2O_5$–$3MgO$–$0.5K_2O$–$4.5ZnO$–$6B_2O_3$); Biphasic calcium phosphate (BCP)	Silver (Ag); Copper (Cu);	BG was synthesized by melting in air, and particle sizes of 315–800 μm were produced. The BCP ceramic was synthesized via decomposition of calcium-deficient non-stoichiometric hydroxyapatite by chemical precipitation. The ceramic composite was doped with a silver (Ag) and copper (Cu) by heating the ceramic granules in silver and copper nitrates solution under stirring until complete solution evaporation followed by drying and heat treatment. Samples were steril-ized by autoclaving.	The TEM images of the BCP showed particles have inhomogeneous morphology before and after calcination that is common for multiphase powders. After calcination, the major part of the particles had a size of less than 100 nm.
Zhang *et al.* (2015)	Amorphous calcium phosphate (ACP) nanospheres; Hy-droxyapatite (HA)	Poly (D, L-lactic acid) (PLA)	For the preparation of ACP-PLA and HA-PLA composite nanofibers, the ACP or HA nanospheres were dispersed in tetrahydrofuran (THF) and N, N-dimethylformamide (DMF) under stirring, followed by the addition of PLA and stirring for 12 h. Then, nanofi-bers were manufactured by the electro-spinning technique.	The TEM images showed nanospheres with diameters of 10 ~ 30 nm. The Electron Diffraction (SAED) analysis pattern demonstrated the ACP nanospheres are amorphous in structure, and the HA nanospheres had a length ranging from 50 to 100 nm and diameters in the range of 20 to 30 nm. The ACP-PLA nanofibers showed good morphology with ~280 nm diameter, while HA-PLA nanofibers presented good morphology, ~350 nm diameter, and rough surface.
Zhou *et al.* (2015)	Nano-hydro-xyapatite (nHA);	Coralline (coral) Recombinant human vascular endothelial growth factor (rhVEGF$_{165}$)	The nHA/coral scaffolds were supplied by Beijing YHJ Science and Trade Co., Ltd and sterilized by γ-irradiation. For the soak loading of the nHA/coral scaffolds, the growth factor rhVEGF$_{165}$ was dissolved in sterile saline in aseptic conditions, and the scaffolds were incubated with 0.25 mL of 12 μg/mL rhVEGF$_{165}$ solution.	SEM showed pores size of 57 to 164 μm. Inside the sample, the macropores were interconnected, and these have diameters from 107 to 550 μm.

►►

Table 2. Bioactive nanoceramic, composite material, the method for scaffold manufacturing and physicochemical characteristics of nanoceramic materials (conc.)

Razavi et al. (2014)	Silicate bioactive akermanite ($Ca_2MgSi_2O_7$)	AZ91 magnesium alloy	The PEO was conducted at 60 V for 30 min, using an electrolyte solution composed of 200 g/L NaOH and 200 g/L Na_2SiO_3, the AZ91 magnesium alloy sample as the anode electrode, and a stainless-steel rectangular plate as the cathode electrode. Then, electrophoretic deposition (EPD) was performed at 100 V for 3 min with a suspension of 10 g akermanite powders and 100 mL of methanol, and the prepared PEO sample and graphite as the cathode and anode, respectively.	The laser scanning microscopy image indicating the microstructure of AZ91 magnesium alloy with an average grain size of 55 ± 10 mm and the average size of the akermanite nanoparticles was 70 ± 20 nm with agglomerative morphologies and irregular shapes. Akermanite/ PEO coating was rough and porous surface, with 50–500 mm islands with a height difference of 100–150, and also small submicron islands of 7 and 11 mm.
Wang et al. (2014)	Nano-calcium phosphate ceramic	Gelatin	The calcium nitrate solution was dissolved in deionized water and methanol and exposed to the atmosphere caused by ammonium carbonate to allow calcium carbonate to grow into the polyurethane foam scaffold at the gas/liquid interface. After that, it was taken out and rinsed with deionized water and hydrothermally treated using an aqueous solution mixture of $(NH_4)_2HPO_4$ and K_2HPO_4 in a Teflon-lined autoclave and sintered at 850 °C for 5 h.	Scaffolds containing gelatin had primary structures of microspheres with a diameter range of 1–2 mm, and secondary ones of 10–25 mm diameters. SEM images depicted the pore walls of the scaffolds with a size of about 1–10 μm. After sintering, the mean pore size for gelatin-containing scaffolds was 368 ± 85 μm.
Zhou et al. (2014)	Amorphous calcium phosphate (CaP) nanospheres	Polylactide (PLA); Tantalum (TA)	Equal weights of CaP nanospheres PLA were mixed in acetone and treated under ultrasonic and magnetic stirring. For the coating process, the TA scaffolds were put into the above CaP-PLA solution and treated under ultrasound, and dried on filter papers.	TEM images showed diameters of CaP nanospheres from 10 to 30 nm. The XRD pattern of CaP nanospheres exhibits no discernable peak of crystalline CaP but a characteristic hump indicating an amorphous phase.
Wang et al. (2013)	Nano-hydroxyapatite (nHA)	Poly (lactic-co-glycolic acid) (PLGA)	The porous PLGA scaffolds were prepared using the room temperature molding/particle leaching method. Oxygen plasma pretreatment was employed. In order to accelerate the HA formation, the scaffolds were immersed in the modified simulated body fluids (SBF) and vacuumed to ensure that pores were filled with the solution. The coated porous scaffolds were rinsed in ion-free water, desiccated, and kept in a vacuum dryer.	The interior pore surfaces of scaffolds were visualized by FE-SEM and exhibited a interconnected 3D structure with pore diameters in the range from 300–450 μm. The thickness of the HA slice was about 50 nm, the width was 400–1000 nm, and the HA slices were closely packed.
Reddy et al. (2012)	Hydroxyapatite (HA); β -tricalcium phosphate (β -TCP)	Mesenchymal stem cells (MSCs)	The scaffolds were prepared by polymer matrix mediated synthesis method, in a narrow range of Ca/P ratios by polymer matrix with a systematic variation in the ratio of H to β -TCP, which gave a Ca/P molar ratio of 1.62 for bioceramic P1, 1.60 for P2 and 1.58 for P3. MSC was cultured on the nanoceramic coated dishes.	TEM images showed the bioceramics P1, P2, and P3 exhibits average size of ~21 nm, ~23 nm, and ~32 nm nanoparticles, respectively.
Yang et al. (2012)	Hydroxyapatite (HA) nanoparticles	Polyglycolic acid (PGA)	PGA meshes were coated with HA nanoparticles by immersing the scaffolds in a Tris buffer solution containing 3,4-dihydroxyphenylalanine (DOPA) (2 mg/mL) only (16 himmersion), HA nanoparticles (20 mg/mL) only (16 -himmersion), or DOPA/HA mixture (8, 16, and 24 h).	TEM showed that the HA-DOPA-PGA scaffolds particles' size was ~ 20 to 50 nm wide and 100 to 200 nm long. The EDS analysis showed an increasing tendency for HA nanoparticles to adhere to the scaffold surface during the immersion time.
Huber et al. (2007)	OSTIM® (resorbable pure hydroxyapatite); CERABONE® (solid hydroxyapatite ceramic)	–	The bioceramics were purchased commercially.	CERABONE® had a mean pore diameter of 800 μm and a range of 100–1500 μm.

Table 3. *In vivo* analysis and overall results.

Author	Nanomaterials	Groups	Analysis	Overall results
Dasgupta *et al.* (2019)	58SBioglass (GCB)/ tricalcium phosphate (GCT)/ hydroxyapatite (GCH)	GCB, GCT, GCH	X-ray, histology, and fluorochrome labeling	GCB group showed complete material degradation, a higher number of blood vessels, and a higher amount of bone formation compared to the other groups.
Chalisserry *et al.* (2019)	nHA/Simvastatin (SIM)	nHA, nHA-SIM	MicroCT, histology, Histomorphometry	Bone volume and bone mineral density were higher in nHA-SIM group than in the control group. The nHA-SIM group also presented faster degradation than nHA group
Kazemi *et al.* (2019)	TRI-CALCIT® HACP/ TEXTILE HI-TEC/ Mesenchymal stem cells (MSC)	Untreated Scaffold, MSC-scaffold, Granule	Micro-CT, Histology, Immunohistochemistry, Histomorphometry	The MSC-scaffold group almost healed after 2 months, providing enhanced mechanical properties with higher bone volume, less fibrous connective tissue, and immunoexpression of OCN compared to other groups.
Liang *et al.* (2019)	Gold (Au)-mesoporous silica-chitosan (MSNs)	Chitosan scaffold, MSNs, Au-MSN	micro-CT, Morphometry, Histology, Immunohistochemistry	Au-MSN promoted higher and accelerated bone formation, higher bone mineral density, and less fibrous tissue compared with MSNs and C scaffolds.
Rogowska-Tylman *et al.* (2019)	Nanohydroxyapatite sonocoate scaffold	nHAP-coated PCL, uncoated β-TCP PCL, nHAP-coated β-TCP	Histology, Morphometry, and Immunohistochemistry	nHAP-coated β-TCP scaffold promoted a higher volume of new bone tissue after three months compared to other groups. nHAP-coated β-TCP showed favorable results regarding osteogenic markers and inflammatory factors detected in bone tissue.
Singh *et al.* (2019)	Chitosan(CH)/ chondroitin sulfate (CS)/nano-Bioglass (nBG)	Untreated, CH/CS/8nBG	Histology	CH/CS/8nBG enhanced bone formation with uniform and dense collagen deposition, and after 24 weeks defect was completely filled with mineralized bone tissue. Untreated defects presented fibrous connective tissue with poor bone formation.
Lisboa-Filho *et al.* (2018)	BioGran®/Raloxifene	BioGran®, BioGran®/Raloxifene (90:10), BioGran®/Raloxifene (80:20)	Micro-CT	Bone volume and trabecular number were lower in BioGran®/Raloxifene (90:10) group compared with the other two. Trabecular thickness did not differ among groups, while trabecular separation was higher in BioGran®/Raloxifene (90:10).
Mabrouk *et al.* (2018)	Copper (Cu) -calcium silicate nanoparticles	Cu-doped calcium silicate nanoparticles (0%; 1%, 3%; 5%)	X-ray and Histology	Healing enhanced with increasing levels of Cu-doped calcium nanoparticles. Great rigidity and resistance to fracture were found in 3 and 5% groups. 5% group presented higher bone mineral density, higher bone healing, and angiogenic effect than the other groups.

►►

Table 3. *In vivo* analysis and overall results (cont.).

Rezaei *et al.* (2018)	Nanosize-Bicalcium Phosphate (BCP)	Commercial BCP, Untreated control, Nano-sized BCP	Histology and Histomorphometry	Nano-sized BCP produced no chronic inflammation or foreign body reaction and increased bone regeneration and higher bone formation after 8 weeks compared to the blank group, and similar to commercial BCP.
Zhang *et al.* (2018)	Macro/microporous nano-bioglass/polyetheretherketone	micro-macroporous polyetheretherketone (mPK),bioglass/polyetheretherketone composite (PBC), micro-nano-bioglass/polyetheretherketone (mPBC),hinokitiol loaded mPBC (dmBPC)	Micro-CT, Histology, and Immuno-histochemistry	mBPC and dmBPC groups presented higher bone formation compared to PBC and PK groups. mBPC and dmBPC promoted BMP-2 expression after 3 months, compared with BPC and mPK.
Shao *et al.* (2017)	TCP/ Wollastonite (Csi)/ Mg, and bredigite (Bred)	TCP, CSi, CSi-Mg10 Bred	X-ray, Macroscopy, microCT, Histology, and Histomorphometry	From week 8 to 16, all groups increased radiodensity (suggesting mineralization). No signs of inflammation, necrosis, or infection were macroscopically detected for all groups, and well-organized calluses covered the implants' whole surface. For the CSI-Mg10 group, lower bone volume was detected at week 8, but the highest levels were observed at week 16, compared with the other groups.
Zhu *et al.* (2017)	BCP	micro/nano hybrid-structured BCP (hBCP), BCP	micro-CT, Histology, and mechanical test	hBCP group showed a better integration with host bone tissue. Bone to material ratio was higher for hBCP group compared with BCP group. Both groups demonstrated good bone integration and osteoconductivity. hBCP also had improved mechanical properties (maximum load but not stiffness) when compared to BCP group.
Ahmad-zadeh *et al.* (2016)	carbonate-zinc-magnesium substituted hydroxyapatite (CZM-HA)	CZM-HÁ and HA	Micro-CT, X-ray, Histology and SEM-EDX and Histomorphometry	After 4 weeks CZM-HA graft was degraded entirely with higher newly formed bone tissue formation compared with the other groups, and no evidence of rejection. High levels of mineralization in the CZM-HA group were also found.
Bennett *et al.* (2016)	poly(D,L-lactide-co-glycolide)/a-tricalcium phosphate	PLGA, PLGA/α-TCP microcomposite, PLGA/α –TCP nanocomposite	X-ray and Histology	Bone formation and implant degradation were similar for all groups. Nanocomposite implants degraded more slowly than microcomposite implants.
Johari *et al.* (2016)	Osteoblasts/bioglass/gelatin	Untreated defect, Bioglass/gelatin scaffold, and Osteoblasts/bioglass/gelatin scaffold	Histology, Histomorphometry, and Immunohistochemistry	Osteoblasts/bioglass/gelatin scaffold produced higher bone formation, lamellar bone formation, collagen type I deposition, and OCN expression after 90 days.

►►

Table 3. *In vivo* analysis and overall results (cont.).

Sun *et al.* (2016)	Porous nHA scaffolds/ peptide 28 (P28)/BMP-2	Untreated defect, nHA, nHA-P28, and nHA-BMP-2	Micro-CT, Histological.	P28 and BMP-2 loaded scaffolds promoted the higher bone formation and higher bone mineral density in critical sized bone defects. These groups also presented osteocytes, osteoid, and blood vessel formation in the material interspace after 6 and 12 weeks. In control groups, loose connective and granulation tissue was observed after 6 weeks.
Ardeshiry-lajim *et al.* (2015)	Nano Bioglass coated (nBG)/ polyethersulphone (PES)	PES, and nBG-PES	X-ray, Micro-CT, and Histology	Higher amounts of bone formation in nBG-PES implanted group. nBG-PES also showed higher collagen deposition after 8 weeks.
Dhivya *et al.* (2015)	zinc-doped chitosan (Zn-CS)/ nanohydroxyapatite (nHAp/β-glycerophosphate (β-GP) hydrogels	Untreated defects, Zn-CS/β-GP, and Zn-CS/nHAp/β-GP	X-Ray and Histology	Zn-CS/nHAp/β-GP produced higher bone formation, better defect closure, and collagen deposition compared to other groups.
Du *et al.* (2015)	nHA/ VEGF/ coral blocks	nHA/coral blocks and nHA/ VEGF/ coral blocks	Histology, Histomorphometry, and Immunohistochemistry	New bone formation in nHA/VEGF/coral group was slightly greater than those of the nHA/coral group. nHA/ VEGF/coral blocks showed a higher density of blood vessels than nHA/coral blocks after 3 weeks, but similar values were detected for both groups at week 8.
Hu *et al.* (2015)	Porous biphasic calcium phosphate ceramics (BCP)/ nHA/ MSCs	BCP, BCP/nHA, BCP/MSCs, and BCP/nHA/MSCs	Mechanical Testing, Histology, Histomorphometry, and Immunohistochemistry	BCP/nHA/MSCs and BCP/MSCs presented increased mechanical strength than BCP/nHA and BCP groups. BCP/nHA/MSCs showed a higher amount of bone tissue formation and immunoexpression of BMP-2 compared to other groups.
Lysenko *et al.* (2015)	Silver/Copper (Ag/Cu) Bioactiveglass/ BCP (BCC)	Intact animals, untreated defect, BCC3 (BCC doped with Ag 1/ Cu 0.5 at.%), and BCC (undoped)	Histology and Specific ions and proteins quantification in bone	BCC and BCC3 stimulated osteogenesis, mainly affecting the mineralization function. However, silver- and copper-doping did not improve bone defect reparation in comparison with BCC (undoped).
Zhang *et al.* (2015)	amorphous calcium phosphate (ACP) nanospheres/ hydroxyapatite (HA) nanorods- poly(D,L-lactic acid) (PLA)	Untreated defect, ACP-PLA, and HA-PLA	Histology	The collagen constituent in bone defects in the composite treated groups was more prominent than the untreated group.
Razavi *et al.* (2014)	Mg alloy (AZ91)/ Akermanite/ plasma electrolytic oxidation (Peo)	AZ91, PEO, Akermanite/PEO	X-ray and Histology	Akermanite/PEO coated group had few hydrogen bubbles due to material degradation, more bone formation, and less inflammatory response compared with the other groups.

►►

Table 3. *In vivo* analysis and overall results (conc.).

Wang *et al.* (2014)	Calcium Phosphate	Porous Calcium Phosphate (PCP) and Scaffold	X-ray and Histology	PCP scaffold stimulated a high-density tissue extended toward the central defect area. PCP scaffolds also induced material resorption and proportional bone formation: in 12 weeks, the whole scaffold was almost completely degraded and ossified.
Zhou *et al.* (2014)	Vasoendothelial Growth Factor (VEGF)/ Transforming Growth Factor-β (TGF-β)/ calcium phosphate (CaP)- polylactide (PLA) coated Tantalum (Ta)	Untreated defect, VEGF/TGF-β/CaP-PLA coated Ta	Histology	VEGF/TGF-β/CaP-PLA coated Ta scaffold produced increased bone formation compared to controls after 12 weeks.
Wang *et al.* (2013)	nHA/Poly(lactic-co-glycolic acid) (PLGA) seeded with BMSCs	BMSCs/PLGA, and BMSCs/nHA-PLGA	Micro-CT, X-ray, Biomechanical test, Histology and Fluo-rochrome labeling	BMSCs/nHA-PLGA group produced higher bone formation and bone mineral density, mechanical properties of the new bone improvement, and higher bone regeneration rate after 12 weeks, compared with BMSCs/PLGA group.

Table 4. Summary of findings: nanoceramic materials compared to control/sham.

Nanomaterials and bone healing										
Out-come	Limita-tions	Incon-sistency	Indirect-ness	Impre-cision	Publica-tions Bias	Trials	Inter-vention (n)	Compa-rison (n)	Signifi-cant dif-ference	GRADE level of evidence
Intervention: Nanomaterials x control/sham										
						Dasgup-ta et al. 2019	6^c	6^c	Yes	
						Kazemi et al. 2019	10^c	10^c	Yes	
						Liang et al. 2019	6^d	6^d	Yes	
						Mabrouk et al. 2018	6^d	6^d	Yes	
						Rezaei et al. 2018	10^d	10^d	Yes	
						Zhang et al. 2018	3^c	3^c	Yes	
						Zhu et al. 2017	6^a	6^a	Yes	
						Ahmad-zadeh et al. 2016	3^c	3^c	Yes	
						Bennet et al. 2016	9^b	9^b	Yes	
						Johari et al. 2016	15^d	15^d	Yes	
						Sun et al. 2016	4^d	4^d	Yes	
						Ar-deshiry-lajimi et al.2015	10^d	10^d	Yes	
						Dhivva et al. 2015	6^d	6^d	Yes	
						Hu et al. 2015	5^c	5^c	Yes	

►►

Table 4. Summary of findings: nanoceramic materials compared to control/sham (conc.)

						Lysenko et al. 2015	16[d]	8[d]	Yes	
						Reddy et al. 2012	3d	3[d]	Yes	
						Huber et al. 2007	8[c]	8[c]	Yes	
	Serious	No	No	Serious	Undetected					Modera-te**

Discussion

The present study demonstrated the effects of different types of ceramic materials, at a nanosize scale, for bone tissue engineering applications. It was possible to observe that, in most of the studies, HA was the choosen nanoceramic material used[30,31,33,38,39,41,46,48]. Moreover, calcium phosphate was used by 3 studies[26,54,62] and bioactive glass was used by 2 studies[25,40]. It is important to highlight that the materials were used isolated or combined with other materials such as chitosan30,40, gelatin[30,32,49], PVA[28,33,37], condroitan sulfate[40], PCL[41], PLGA[34,55,] PES[44], β-GP[48], PLA[39,56], coral[53], PGA[52] and metals[45,50].

As previously described, nanoceramic materials, especially HA, TCP and BG, have been profusely investigated as biomaterials mainly due to their capability to bond directly to living tissue after implantation, especially in bone defects, stimulating tissue ingrowth[61–68]. In addition, nanoceramic materials have also emerged as an optimized alternative to be used as bone grafts, combining the positive biological properties of ceramics with the superior strength and toughness of the nanomaterials[69].

From the papers analyzed in the present review, it is possible to observe that nano-HA was able of shortening the process of bone healing due to its osteocondutive properties and enhanced solubility, being able of increasing the calcium ion concentration[41,70]. Moreover, 5 studies explored the osteogenic behavior of calcium phosphate as nanoceramic material[26,32,54–56], whereas the calcium silicate nanoceramic was employed in the studies of Shao et al.[28] (2018) and Mabrouk et al.[50] (2018). Similarly, nano-CP and nano-BTCP have been used by many authors, also demonstrating optimized results in the process of bone healing compared to micro-B--TCP71–73. Nano-BG was also used by 5 authors or with the combination of other materials such as HA and β-TCP[37,40,44,49,63]. Researchers have pointed out that nano-BG has superiority over micro-BG in repairing bone defects[71,72]. For example, Nosouhian et al.[75] (2019) showed that the nano-BG produced a higher rate of bone formation compared to nano-HA in an experimental model of bone defects.

Moreover, nanoceramic materials also have been used in association with other materials, mainly synthetic biopolymers[34,37,39,41,44,52,55,63] and natural polymers[30,32,40,49]. The introduction of polymers to nanoceramic materials for manufacturing scaffolds aims to improve the mechanical and biological properties76. Metals are also materials used for nanoceramic composite manufacturing, providing a series of advantages such as stability and improved mechanical properties[45,48,50,51,57]. In addition, among the selected articles, 3 of them fabricated scaffolds

with nanoceramic-synthetic biopolymer-metal[28,33,56]. Previous studies demonstrated that combining metal ions-doped nanoceramic materials with bioactive polymers significantly accelerated the healing in experimental models of bone defects due to the physicochemical similarities between the graft compositions and bone tissue[33]. In addition, 2 studies employed nanoceramic materials combined with commercial drugs, simvastatin, an inhibitor of cholesterol synthesis Chalisserry et al.[38] (2019) and raloxifene, a selective modulator of estrogen receptors[25]. In the study of Lisboa-Filho et al.[25] (2018), the biological effects of raloxifene combined with BioGran® in the repair of critical bone defects in the calvaria of rats were observed. The incorporation of raloxifene in the range of 80/20 mass concentration showed to be the most effective for bone formation. This suggests the possibility of combined antiresorptive medications with BG in order to improve bone regeneration. Chalisserry et al.[38] (2019) observed a significant enhancement of bone formation in the rabbit femoral condyle due to the favorable degradation rate of drug delivery system made of nHA scaffolds loaded with a gradual release of simvastatin, that promoted significantly high bone regeneration in a critical size defect in rabbit femoral condyle

Interestingly, Zhou et al.[56] (2014) and Sun et al.[46] (2016), loaded nanoceramic scaffolds with recombinant Human VEGF and bone morphogenic protein (BMP-2)-related peptide (P28), respectively. The authors suggested that the combination of growth factors results in angiogenesis and bone formation more readily than a single factor alone. Due to this observation, as a future trend the development of multilayer biodegradable composite scaffold to use different combination of growth factors must be investigated to optimize bone tissue healing using nanoceramic materials.

Also, different methods for manufacturing the scaffolds from nanoceramic materials were applied. The electrospinning technique is a unique approach using electrostatic forces to produce fine fibers from polymer solutions or melts with a thinner diameter (from nanometer to micrometer) and a larger surface area, in comparison to those obtained from conventional spinning processes[77]. In addition, the leaching method is also an efficient method for scaffold manufacturing, combining different methods such as casting, compression molding, and extrusion[78]. The replication method is a process that involves the coating of open-cell polymeric foam, with ceramic slurry followed by burning-out of polymeric foam producing ceramic foam with the vast majority of open cell foam microstructure[79]. Also, the sintered process consisted of heating the material

at high temperatures (between 1100 and 1400 °C) Sadowska et al.[80](2017). Furthermore, Lisboa-Filho et al.[25] (2018) and Rogowska-Tylman et al.[41] (2019) applied the sonochemical and ultra-sonification methods. The sonochemical technique also known as ultra-sonification consists of the use of a ultra-sound probe and a signal generation[81].

Moreover, characterization of the scaffolds was performed by mainly FTIR, SEM and TEM analysis. The FTIR spectroscopy analysis demonstrated the chemical characterization of the biomaterials; for example, it depicted the hydroxyl, phosphate, and carbonate groups related to BCP[26], or the functional groups of hydroxyapatite, that include PO_4^{3-} (PO), $OH-$ (O-H) and CO_3^{2-} [31,33]. The SEM evaluation showed a range of 100–500 μm[37], 170 μm – 540 μm[40], 200 to 500 μm and porosity about 85%[49]. TEM analysis demonstrated particle size around 20 to 50 nm[52] and 10 to 30 nm[56] and rounded grains with a diameter about 50 nm can be observed in the work of Mabrouk et al.[50] Although the optimal pore size for osteoblast activity in tissue engineered scaffolds remains a controversial question, in general, scaffolds with pore sizes of about 20 to 1500 nm have been used[82].

Considering the in vivo results, all the studies demonstrated a stimulatory effect on the process of bone healing after the treatment with the different nanoceramic materials. Micro-CT has shown that higher bone ingrowth and higher density were observed in the region of the defect after the nanoscaffold implantation[46–48,50,54,55,57,83,84,30,32–34,37,38,44,45]. Also, histology demonstrated that all kinds of bioceramics degraded over time, releasing space for newly formed bone ingrowth and consequently, a higher amount of newly formed bone was also observed [26,28,44–50,52,54,55,31,56,57,63,32–34,37,39,41,42]. Many studies have demonstrated that ceramic bone grafts can attract and stimulate cells at the region of the fractures and also forming a hydroxycarbonate apatite (HCA) film with bone tissue, mimicking the natural interface the restoration of bone and stimulating tissue repair [19,85]

Moreover, neoangiogenesis and higher immunostaining of osteogenic markers, such as OCN[37,41,49], BMP-2[31,41,46], OPG[41], OP[41], VEGF[53], MMP2[41], Col-1[41], and IL1[41], were observed in the nanoceramic material treated animals. OCN is a hormone-like peptide secreted by osteoblasts[86], related to osteoblasts differentiation[36,87] and bone remodeling process[88]. In addition, BMP-2 is also related to an increase in OCN expression[89] and OPG is responsible for regulating the remodeling/resorption process. Also, VEGF is a key factor for angiogenesis, involved in new blood vessel formation. Finally, Col-1 is a representative marker of ossification and leads to the process of

callus remodeling in the resorption stage[90–92]. It is important to emphasize that the positive effects of nanoceramic materials on the immunostaining of the osteogenic markers may be related to the ions dissolution from the ceramics and consequently, could have contributed to the improved process of healing in the treated animals.

Taking all the data together, nanoceramic materials, used isolated or combined with other materials or drugs constituted an efficient therapeutical intervention, with a huge potential to be used in the area of bone tissue engineering.

Conclusion

In conclusion, this review demonstrates that nanoceramic materials, can be successfully used for manufacturing scaffolds using different techniques. Also, the nanoceramic materials were able of stimulating tissue ingrowth and accelerating the process of bone healing in animal studies. However, further studies are needed, especially at the clinical setting, with the aim of evaluating the efficiency and safety of nanoceramic materials to be used as bone grafts.

Ethical Approval
Not Applicable.

Informed Consent
Not Applicable.

Funding

Conflict of interest statement
On behalf of all authors, the corresponding author states that there is no conflict of interest.

References

[1]. Qasim M, Chae DS, Lee NY. Bioengineering strategies for bone and cartilage tissue regeneration using growth factors and stem cells. Journal of Biomedical Materials Research - Part A 2020; 108: 394–411.

[2]. Wang W, Yeung KWK. Bone grafts and biomaterials substitutes for bone defect repair: A review. Bioact Mater 2017; 2: 224–247.

[3]. Osorio CC, Escobar LM, González MC, et al. Evaluation of density, volume, height and rate of bone resorption of substitutes of autologous bone grafts for the repair of alveolar clefts in humans: A systematic review. Heliyon; 6. Epub ahead of print 2020. DOI: 10.1016/j.heliyon.2020.e04646.

[4]. Wiese A, Pape HC. Bone Defects Caused by High-energy Injuries, Bone Loss, Infected Nonunions, and

Nonunions. Orthop Clin North Am 2010; 41: 1–4.

[5]. Li C, Wang GX, Zhang Z, et al. Biocompatibility and in vivo osteogenic capability of novel bone tissue engineering scaffold A-W-MGC/CS. J Orthop Surg Res 2014; 9: 100.

[6]. Oryan A, Monazzah S, Bigham-Sadegh A. Bone injury and fracture healing biology. Biomed Environ Sci. Epub ahead of print 2015. DOI: 10.3967/bes2015.006.

[7]. Díaz ECG, Shih YR V., Nakasaki M, et al. Mineralized Biomaterials Mediated Repair of Bone Defects Through Endogenous Cells. Tissue Eng - Part A 2018; 24: 1148–1156.

[8]. Alexander Hofmann, MD, PhD, Stanislav Gorbulev, PhD, Thorsten Guehring, MD, PhD, Arndt Peter Schulz, MD P, Rupert Schupfner, MD, Michael Raschke, MD, PhD, Stefan Huber-Wagner, MD, PhD, Pol Maria Rommens, MD P. Autologous Iliac Bone Graft Compared with Biphasic Hydroxyapatite and Calcium Sulfate Cement for the Treatment ofBone Defects in Tibial Plateau Fractures. 2019; 1–9.

[9]. Fernandez de Grado G, Keller L, Idoux-Gillet Y, et al. Bone substitutes: a review of their characteristics, clinical use, and perspectives for large bone defects management. J Tissue Eng; 9. Epub ahead of print 2018. DOI: 10.1177/2041731418776819.

[10]. Chen FM, Liu X. Advancing biomaterials of human origin for tissue engineering. Prog Polym Sci 2016; 53: 86–168.

[11]. Diaz-Rodriguez P, Sánchez M, Landin M. Drug-loaded biomimetic ceramics for tissue engineering. Pharmaceutics 2018; 10: 1–20.

[12]. Ginebra MP, Espanol M, Maazouz Y, et al. Bioceramics and bone healing. EFORT Open Rev 2018; 3: 173–183.

[13]. Zhang H, Zhou Y, Yu N, et al. Construction of vascularized tissue-engineered bone with polylysine-modified coral hydroxyapatite and a double cell-sheet complex to repair a large radius bone defect in rabbits. Acta Biomater 2019; 91: 82–98.

[14]. Zhou K, Yu P, Shi X, et al. Hierarchically Porous Hydroxyapatite Hybrid Scaffold Incorporated with Reduced Graphene Oxide for Rapid Bone Ingrowth and Repair. ACS Nano 2019; 13: 9595–9606.

[15]. Coelho CC, Grenho L, Gomes PS, et al. Nano-hydroxyapatite in oral care cosmetics: characterization and cytotoxicity assessment. Sci Rep 2019; 9: 1–10.

[16]. Rh. Owen G, Dard M, Larjava H. Hydoxyapatite/beta-tricalcium phosphate biphasic ceramics as regenerative material for the repair of complex bone defects. J Biomed Mater Res - Part B Appl Biomater 2018; 106: 2493–2512.

[17]. Li T, Peng M, Yang Z, et al. 3D-printed IFN-γ-loading calcium silicate-β-tricalcium phosphate scaffold sequentially activates M1 and M2 polarization of macrophages to promote vascularization of tissue engineering bone. Acta Biomater 2018; 71: 96–107.

[18]. Larry L H, Julia M P. Third-generation biomedical materials. Science (80-) 2002; 295: 1014–1017.

[19]. Hench LL. The story of Bioglass. J Mater Sci Mater Med 2006; 17: 967–978.

[20]. Chaair H, Labjar H, Britel O. Synthèse du phosphate tricalcique-β. Morphologie 2017; 101: 120–124.

[21]. Campana V, Milano G, Pagano E, et al. Bone substitutes in orthopaedic surgery: from basic science to clinical practice. J Mater Sci Mater Med 2014; 25: 2445–2461.

[22]. Subramaniam S, Fang YH, Sivasubramanian S, et al. Hydroxyapatite-calcium sulfate-hyaluronic acid composite encapsulated with collagenase as bone substitute for alveolar bone regeneration. Biomaterials 2016; 74: 99–108.

[23]. Ain Q, Zeeshan M, Khan S, et al. Biomimetic hydroxyapatite as potential polymeric nanocarrier for the treatment of rheumatoid arthritis. J Biomed Mater Res - Part A 2019; 107: 2595–2600.

[24]. Prowans P, Kowalczyk R, Wiszniewska B, et al. Bone Healing in the Presence of a Biodegradable PBS-DLA Copolyester and Its Composite Containing Hydroxyapatite. ACS Omega 2019; 4: 19765–19771.

[25]. Lisboa-Filho PN, Gomes-Ferreira PHS, Batista FRS, et al. Bone repair with raloxifene and bioglass nanoceramic composite in animal experiment. Connect Tissue Res 2018; 59: 97–101.

[26]. Rezaei M, Farhadian M, Rashidi AM, et al. Nano-biphasic calcium phosphate ceramic for the repair of bone defects. J Craniofac Surg 2018; 29: e543–e548.

[27]. McMahon RE, Wang L, Skoracki R, et al. Development of nanomaterials for bone repair and regeneration. J Biomed Mater Res - Part B Appl Biomater 2013; 101 B: 387–397.

[28]. Shao H, Sun M, Zhang F, et al. Custom Repair of Mandibular Bone Defects with 3D Printed Bioceramic Scaffolds. J Dent Res 2018; 97: 68–76.

[29]. de Vries FEE, Reeskamp LF, van Ruler O, et al. Systematic review: pharmacotherapy for high-output enterostomies or enteral fistulas. Aliment Pharmacol Ther 2017; 46: 266–273.

[30]. Dasgupta S, Maji K, Nandi SK. Investigating the mechanical, physiochemical and osteogenic properties in gelatin-chitosan-bioactive nanoceramic composite scaffolds for bone tissue regeneration: In vitro and in vivo. Mater Sci Eng C 2019; 94: 713–728.

[31]. Hu J, Yang Z, Zhou Y, et al. Porous biphasic calcium phosphate ceramics coated with nano-hydroxyapatite and seeded with mesenchymal stem cells for reconstruction of radius segmental defects in rabbits. J Mater Sci Mater Med; 26. Epub ahead of print 2015. DOI: 10.1007/s10856-015-5590-4.

[32]. Wang J, Yan H, Chen T, et al. Porous nanoapatite scaffolds synthesized using an approach of interfacial

mineralization reaction and their bioactivity. J Biomed Mater Res - Part B Appl Biomater 2014; 102: 1749–1761.

[33]. Ahmadzadeh E, Talebnia F, Tabatabaei M, et al. Osteoconductive composite graft based on bacterial synthesized hydroxyapatite nanoparticles doped with different ions: From synthesis to in vivo studies. Nanomedicine Nanotechnology, Biol Med 2016; 12: 1387–1395.

[34]. Wang DX, He Y, Bi L, et al. Enhancing the bioactivity of Poly(lactic-co-glycolic acid) scaffold with a nano-hydroxyapatite coating for the treatment of segmental bone defect in a rabbit model. Int J Nanomedicine 2013; 8: 1855–1865.

[35]. Hou G, Zhou F, Guo Y, et al. In vivo study of a bioactive nanoparticle-gelatin composite scaffold for bone defect repair in rabbits. J Mater Sci Mater Med; 28. Epub ahead of print 2017. DOI: 10.1007/s10856-017-5991-7.

[36]. Wang J, Wang M, Chen F, et al. Nano-hydroxyapatite coating promotes porous calcium phosphate ceramic-induced osteogenesis via BMP/SMAD signaling pathway. Int J Nanomedicine 2019; 14: 7987–8000.

[37]. Kazemi M, Dehghan MM, Azami M. Biological evaluation of porous nanocomposite scaffolds based on strontium substituted β-TCP and bioactive glass: An in vitro and in vivo study. Mater Sci Eng C 2019; 105: 110071.

[38]. Chalisserry EP, Nam SY, Anil S. Simvastatin Loaded Nano Hydroxyapatite in Bone Regeneration: A Study in the Rabbit Femoral Condyle. Curr Drug Deliv 2019; 16: 530–537.

[39]. Zhang H, Fu QW, Sun TW, et al. Amorphous calcium phosphate, hydroxyapatite and poly(d,l-lactic acid) composite nanofibers: Electrospinning preparation, mineralization and in vivo bone defect repair. Elsevier B.V., 2015. Epub ahead of print 2015. DOI: 10.1016/j.colsurfb.2015.08.015.

[40]. Singh BN, Veeresh V, Mallick SP, et al. Design and evaluation of chitosan/chondroitin sulfate/nano-bioglass based composite scaffold for bone tissue engineering. Int J Biol Macromol 2019; 133: 817–830.

[41]. Rogowska-Tylman J, Locs J, Salma I, et al. In vivo and in vitro study of a novel nanohydroxyapatite sonocoated scaffolds for enhanced bone regeneration. Mater Sci Eng C 2019; 99: 669–684.

[42]. Huber FX, Berger I, McArthur N, et al. Evaluation of a novel nanocrystalline hydroxyapatite paste and a solid hydroxyapatite ceramic for the treatment of critical size bone defects (CSD) in rabbits. J Mater Sci Mater Med 2008; 19: 33–38.

[43]. Ghorbanian L, Emadi R, Razavi SM, et al. Fabrication and characterization of novel diopside/silk fibroin nanocomposite scaffolds for potential application in maxillofacial bone regeneration. Int J Biol Macromol 2013; 58: 275–280.

[44]. Ardeshirylajimi A, Farhadian S, Adegani FJ, et al. Enhanced osteoconductivity of polyethersulphone nanofibres loaded with bioactive glass nanoparticles in in vitro and in vivo models. Cell Prolif 2015; 48: 455–464.

[45]. Liang H, Jin C, Ma L, et al. Accelerated Bone Regeneration by Gold-Nanoparticle-Loaded Mesoporous Silica through Stimulating Immunomodulation. ACS Appl Mater Interfaces 2019; 11: 41758–41769.

[46]. Sun T, Zhou K, Liu M, et al. Loading of BMP-2-related peptide onto three-dimensional nano-hydroxyapatite scaffolds accelerates mineralization in critical-sized cranial bone defects. J Tissue Eng Regen Med 2018; 12: 864–877.

[47]. Reddy S, Wasnik S, Guha A, et al. Evaluation of nano-biphasic calcium phosphate ceramics for bone tissue engineering applications: In vitro and preliminary in vivo studies. J Biomater Appl 2013; 27: 565–575.

[48]. Dhivya S, Saravanan S, Sastry TP, et al. Nanohydroxyapatite-reinforced chitosan composite hydrogel for bone tissue repair in vitro and in vivo. J Nanobiotechnology 2015; 13: 1–13.

[49]. Johari B, Kadivar M, Lak S, et al. Osteoblast-seeded bioglass/gelatin nanocomposite: A promising bone substitute in critical-size calvarial defect repair in rat. Int J Artif Organs 2016; 39: 524–533.

[50]. Mabrouk M, ElShebiney SA, Kenawy SH, et al. Novel, cost-effective, Cu-doped calcium silicate nanoparticles for bone fracture intervention: Inherent bioactivity and in vivo performance. J Biomed Mater Res - Part B Appl Biomater 2019; 107: 388–399.

[51]. Lysenko O, Dubok O, Borysenko A, et al. The biological properties of the silver- and copper-doped ceramic biomaterial. J Nanoparticle Res; 17. Epub ahead of print 2015. DOI: 10.1007/s11051-015-2971-z.

[52]. Yang HS, Park J, La WG, et al. 3,4-Dihydroxyphenylalanine-assisted hydroxyapatite nanoparticle coating on polymer scaffolds for efficient osteoconduction. Tissue Eng - Part C Methods 2012; 18: 245–251.

[53]. Du B, Liu W, Deng Y, et al. Angiogenesis and bone regeneration of porous nano-hydroxyapatite/coralline blocks coated with rhVEGF165 in critical-size alveolar bone defects in vivo. Int J Nanomedicine 2015; 10: 2555–2565.

[54]. Zhu Y, Zhang K, Zhao R, et al. Bone regeneration with micro/nano hybrid-structured biphasic calcium phosphate bioceramics at segmental bone defect and the induced immunoregulation of MSCs. Biomaterials 2017; 147: 133–144.

[55]. Bennett SM, Arumugam M, Wilberforce S, et al. The effect of particle size on the in vivo degradation of poly(D,L-lactide-co-glycolide)/α-tricalcium phosphate micro- and nanocomposites. Acta Biomater 2016; 45: 340–348.

[56]. Zhou R, Xu W, Chen F, et al. Amorphous calcium phosphate nanospheres/polylactide composite coated tantalum scaffold: Facile preparation, fast biomineralization and subchondral bone defect repair application. Colloids Surfaces B Biointerfaces 2014; 123: 236–245.

[57]. Razavi M, Fathi M, Savabi O, et al. In vivo study of nanostructured akermanite/PEO coating on biodegradable magnesium alloy for biomedical applications. J Biomed Mater Res - Part A 2015; 103: 1798–1808.

[58]. Yang X, Qin L, Liang W, et al. New bone formation and microstructure assessed by combination of confocal laser scanning microscopy and differential interference contrast microscopy. Calcif Tissue Int 2014; 94: 338–347.

[59]. Goswami N, Sharma DK. Structural and optical properties of unannealed and annealed ZnO nanoparticles prepared by a chemical precipitation technique. Phys E Low-Dimensional Syst Nanostructures 2010; 42: 1675–1682.

[60]. Agarwal S, Wendorff JH, Greiner A. Use of electrospinning technique for biomedical applications. Polymer (Guildf) 2008; 49: 5603–5621.

[61]. Guvendiren M, Molde J, Soares RMD, et al. Designing Biomaterials for 3D Printing. ACS Biomater Sci Eng 2016; 2: 1679–1693.

[62]. Yang X, Yang J, Wang L, et al. Pharmaceutical Intermediate-Modified Gold Nanoparticles: Against Multidrug-Resistant Bacteria and Wound-Healing Application via an Electrospun Scaffold. ACS Nano. Epub ahead of print 2017. DOI: 10.1021/acsnano.7b01240.

[63]. Zhang J, Wei W, Yang L, et al. Stimulation of cell responses and bone ingrowth into macro-microporous implants of nano-bioglass/polyetheretherketone composite and enhanced antibacterial activity by release of hinokitiol. Colloids Surfaces B Biointerfaces 2018; 164: 347–357.

[64]. Song W, Sun W, Chen L, et al. In vivo Biocompatibility and Bioactivity of Calcium Silicate-Based Bioceramics in Endodontics. Front Bioeng Biotechnol 2020; 8: 1–17.

[65]. Jitaru S, Hodisan I, Timis L, et al. The use of bioceramics in endodontics - literature review. Clujul Med 2016; 89: 470–473.

[66]. RAGHAVENDRA SS. Biocerm. Bioceram Endod – a Rev 2017; 51: 128–137.

[67]. Alves AMM, de Miranda Fortaleza LM, Filho ALMM, et al. Evaluation of bone repair after application of a norbixin membrane scaffold with and without laser photobiomodulation (λ 780 nm). Lasers Med Sci. Epub ahead of print 2018. DOI: 10.1007/s10103-018-2506-9.

[68]. de Oliveira, N.G.; Araújo, P. R. S.; da Silveira, M. T.; Sobral, A.P. V.; Carvalho M V. Comparison of the biocompatibility of calcium silicate-based materials to mineral trioxide aggregate: Systematic review. Eur J Dent 2019; 11: 192–195.

[69]. Gao C, Deng Y, Feng P, et al. Current progress in bioactive ceramic scaffolds for bone repair and regeneration. Int J Mol Sci 2014; 15: 4714–4732.

[70]. Tian B, Chen W, Yu D, et al. Fabrication of silver nanoparticle-doped hydroxyapatite coatings with oriented block arrays for enhancing bactericidal effect and osteoinductivity. J Mech Behav Biomed Mater 2016; 61: 345–359.

[71]. Gamal AY, Iacono VJ. Mixed Nano/Micro-Sized Calcium Phosphate Composite and EDTA Root Surface Etching Improve Availability of Graft Material in Intrabony Defects: An In vivo Scanning Electron Microscopy Evaluation. J Periodontol 2013; 84: 1730–1739.

[72]. Elrayah A, Zhi W, Feng S, et al. Preparation of micro/nano-structure copper-substituted hydroxyapatite scaffolds with improved angiogenesis capacity for bone regeneration. Materials (Basel); 11. Epub ahead of print 2018. DOI: 10.3390/ma11091516.

[73]. de Melo Pereira D, Eischen-Loges M, Birgani ZT, et al. Proliferation and Osteogenic Differentiation of hMSCs on Biomineralized Collagen. Front Bioeng Biotechnol 2020; 8: 1–16.

[74]. Razavi S, Rismanchian M, Jafari-pozve N, et al. Comparing the Efficacy of Three Different Nano-scale Bone Substitutes: In vivo Study. Adv Biomed Res 2017; 6: 64.

[75]. Nosouhian S, Razavi M, Jafari-Pozve N, et al. Comparative evaluation of hydroxyapatite and nano-bioglass in two forms of conventional micro-and nano-particles in repairing bone defects (an animal study). Indian J Dent Res 2015; 26: 366–371.

[76]. Teixeira KN, Duque TM, Maia HP, et al. Fracture resistance and failure mode of custom-made post-andcores of polyetheretherketone and nano-ceramic composite. Oper Dent 2020; 45: 505–515.

[77]. Bhardwaj N, Kundu SC. Electrospinning: A fascinating fiber fabrication technique. Biotechnol Adv 2010; 28: 325–347.

[78]. Wu L, Jing D, Ding J. A 'room-temperature' injection molding/particulate leaching approach for fabrication of biodegradable three-dimensional porous scaffolds. Biomaterials 2006; 27: 185–191.

[79]. Li X, van Blitterswijk CA, Feng Q, et al. The effect of calcium phosphate microstructure on bone-related cells in vitro. Biomaterials 2008; 29: 3306–3316.

[80]. Sadowska JM, Guillem-Marti J, Montufar EB, et al. Biomimetic versus sintered calcium phosphates: The in vitro behavior of osteoblasts and mesenchymal stem cells. Tissue Eng - Part A 2017; 23: 1297–1309.

[81]. Pokhrel N, Vabbina PK, Pala N. Sonochemistry:

Science and Engineering. Ultrason Sonochem 2016; 29: 104–128.

[82]. Loh QL, Choong C. Three-Dimensional Scaffolds for Tissue Engineering Applications: Role of Porosity and Pore Size. Tissue Eng Part B Rev 2013; 19: 485–502.

[83]. He Y, Dong Y, Cui F, et al. Ectopic osteogenesis and scaffold biodegradation of nano-hydroxyapatite-Chitosan in a rat model. PLoS One 2015; 10: 1–15.

[84]. Yang YQ, Tan YY, Wong R, et al. The role of vascular endothelial growth factor in ossification. Int J Oral Sci 2012; 4: 64–68.

[85]. Hench LL, Jones JR. Bioactive Glasses: Frontiers and Challenges. Front Bioeng Biotechnol 2015; 3: 1–12.

[86]. Price PA, Parthemore JG, Deftos LJ, et al. New Biochemial marker for bone metabolism. Measurement by radioimmunoassay of bone GLA protein in the plasma of normal subjects and patients with bone disease. J Clin Invest 1980; 66: 878–883.

[87]. Abdallah HM, Al-Abd AM, Asaad GF, et al. Isolation of antiosteoporotic compounds from seeds of Sophora japonica. PLoS One 2014; 9: 1–8.

[88]. Li C, Wang Q, Gu X, et al. Porous Se@SiO2 nanocomposite promotes migration and osteogenic differentiation of rat bone marrow mesenchymal stem cell to accelerate bone fracture healing in a rat model. Int J Nanomedicine. Epub ahead of print 2019. DOI: 10.2147/IJN.S202741.

[89]. Huang Z, Ren PG, Ma T, et al. Modulating osteogenesis of mesenchymal stem cells by modifying growth factor availability. Cytokine. Epub ahead of print 2010. DOI: 10.1016/j.cyto.2010.06.002.

[90]. Zhang L, Ke X, Lin L, et al. Systematic evaluation of the osteogenic capacity of low-melting bioactive glass-reinforced 45S5 Bioglass porous scaffolds in rabbit femoral defects. Biomed Mater; 12. Epub ahead of print 2017. DOI: 10.1088/1748-605X/aa6b5c.

[91]. Bharadwaz A, Jayasuriya AC. Osteogenic differentiation cues of the bone morphogenetic protein-9 (BMP-9) and its recent advances in bone tissue regeneration. Mater Sci Eng C; 120. Epub ahead of print 2021. DOI: 10.1016/j.msec.2020.111748.

[92]. Zhou X, von der Mark K, Henry S, et al. Chondrocytes Transdifferentiate into Osteoblasts in Endochondral Bone during Development, Postnatal Growth and Fracture Healing in Mice. PLoS Genet; 10. Epub ahead of print 2014. DOI: 10.1371/journal.pgen.1004820.